Electronic Research Archive

http://www.aimspress.com/journal/era

ERA, 32(1): 686–706.
DOI: 10.3934/era.2024033
Received: 25 September 2023
Revised: 23 December 2023
Accepted: 27 December 2023
Published: 09 January 2024

Research article

The influence of synaptic strength and noise on the robustness of central pattern generator

Feibiao Zhan[1], **Jian Song**[2,3,*] **and Shenquan Liu**[2]

[1] School of Mathematics, Nanjing Audit University, Nanjing 211815, China

[2] School of Mathematics, South China University of Technology, Guangzhou 510640, China

[3] School of Mathematical and Computational Sciences, Massey University, Auckland 4442, New Zealand

* **Correspondence:** Email: masongj_vlp@mail.scut.edu.cn.

Abstract: In this paper, we explore the mechanisms of central pattern generators (CPGs), circuits that can generate rhythmic patterns of motor activity without external input. We study the half-center oscillator, a simple form of CPG circuit consisting of neurons connected by reciprocally inhibitory synapses. We examine the role of asymmetric coupling factors in shaping rhythm activity and how different network topologies contribute to network efficiency. We have discovered that neurons with lower synaptic strength are more susceptible to noise that affects rhythm changes. Our research highlights the importance of asymmetric coupling factors, noise, and other synaptic parameters in shaping the broad regimes of CPG rhythm. Finally, we compare three topology types' regular regimes and provide insights on how to locate the rhythm activity.

Keywords: rhythm activity; topology; noise; robustness; central pattern generator

1. Introduction

Central pattern generator (CPG) is a microcircuit of neuron network that can generate multi-rhythm pattern sequences spontaneously without any external information input [1,2]. It controls motor behaviors such as swimming [3,4], walking, breathing, heartbeat, and more [2,5–7]. Recently, Marder et al. made a well-summarized study about CPG and put forward new insights on small rhythmic circuits [8]. CPG is characterized by the robustness and flexibility of the neuronal network in rhythmic activity.

There have been numerous studies examining the working mechanisms of CPGs from both theoretical and experimental perspectives [9–16]. However, achieving flexibility and robustness in CPGs remains not fully understood. Coordination of motor rhythms can be better achieved through the

connection between CPGs, which may form an attractor. Each attractor determines a rhythmic behavior [17, 18]. Some researchers have proposed a rhythmic pattern for human arm movement, indicating that humans also possess a higher level of CPG in their central nervous system. Research on the reasons for these characteristics of CPGs is still ongoing, and it remains unclear how CPGs achieve the robustness and flexibility required for the collaborative implementation of essential rhythm patterns [19]. Thus, discussion on the rhythmic activity pattern of CPGs is still active [20, 21]. Some models are based on Hodgkin-Huxley (HH) neurons, while others are non-periodic neural oscillation models. Theoretical researchers have revealed the hidden internal mechanisms of CPGs from the perspective of dynamics [13, 22]. Collens et al. have revealed a mutually inhibitory tri-neuron neural network that explains the emergence, disappearance, and stability of neuronal rhythm with the change of synaptic parameters [22]. Lu et al. [23, 24] have studied the synchronization and resonance of small-world networks based on CPGs and proposed integer and fractional models based on the working mechanisms of CPGs. Recent research by Zang and Marder in PNAS (2023) demonstrates that how the spatial morphology of neurons can significantly impact the firing patterns of the CPG circuit [25]. The firing mechanism of neuronal rhythm is known to vary according to several studies [26–28]. However, it is still unclear whether this diversity in neuronal rhythm implies a diversity of CPG circuit function. A crucial question is whether the same CPG circuit can produce multiple motor behaviors, making it multifunctional [29, 30]. The generation of motor behavior depends on the modulation of a variety of motor rhythms, making it necessary and important to study rhythm diversity in order to understand the function of CPG.

Studying small circuits is crucial to understanding CPG. Typically, these circuits are half-center oscillators (HCO), the smallest building unit that consists of groups of neurons that inhibit each other [31, 32]. HCO circuits are considered the easiest to identify. The firing patterns of HCOs may also be influenced by neuronal phase response curves, as indicated in the work by Zang et al. [33]. The synchronization of two neurons has been explored by researchers [34, 35]. They have analyzed how neuronal parameters affect the network activity of HCO, which in turn affects motor control [36]. Researchers have also analyzed the effect of changes in system parameter space on the robustness of the HCO bursting model [37, 38]. Noise, the robustness of HCO, and sensory feedback are closely related [39, 40]. However, the effect of synaptic conductance on HCO rhythm patterns still needs to be analyzed. Inhibition of connection can improve the stability of CPG, and we will explore how changes in the rhythm pattern of HCO and tri-neuron CPG occur with the system parameter regime. We will also examine the effects of synaptic conductance and noise on CPG rhythm patterns.

In this study, we investigate the origin of the flexibility and robustness of CPGs as well as the impact of synaptic conductance on the network rhythm. We examine three different topological modes where each neuron has at least one connection to the other member of the CPG. Our findings demonstrate that diverse rhythm patterns exist in Patterns B and C, as shown in Figure 3. These results are based on the functional characteristics of CPG network structures, which are classified as "open" and "non-open" and were studied by Huerta et al. These findings are also consistent with certain biological principles [41]. Rhythmic motor patterns are associated with diseases such as spinal cord injury and can be easily studied quantitatively. Therefore, the study of CPG rhythm can significantly contribute to the development of disease diagnosis and the advancement of intelligent science. For example, Mader et al. (2001) elaborated that CPG can contribute to the development of new therapeutic methods in the recovery of spinal cord injury and summarized the mechanism process of CPG [1]. The biological

CPG principle and the establishment of spiking neural network [42–45] inspire the development of intelligent science.

The paper is structured as follows. In Section 2, we describe the materials and methods we used in building CPG, including the HH neuron model. Then, in Section 3.1, we illustrate how the rhythm pattern of HCO is regulated by synaptic strength and noise. In Section 3.2, we investigate CPG rhythms in other topologies. Finally, we present the discussion and conclusion in Section 4.

2. Materials and methods

2.1. Neuronal model and dynamics

In our CPG, each interneuron is modeled by a Hodgkin–Huxley (HH) model. This microcircuit captures the dynamics by a single compartment, which is described by the following differential equations [28, 46, 47]:

$$\begin{aligned} C_m\frac{dV}{dt} &= -I_{Na} - I_K - I_{Leak} + I_D, \\ \frac{dn}{dt} &= \frac{n_\infty - n}{\tau_n}, \\ \frac{dQ}{dt} &= \omega + \sqrt{2D}\xi(t). \end{aligned} \tag{2.1}$$

Here, C_m denotes the neural membrane capacitance density ($\mu F/cm^2$); V represents the membrane potential (mV); the gating variable n of activated K^+ channels, denotes the activation probability of potassium ion channels; τ_n is the time constant (ms); $\xi(t)$ is Gaussian white noise; ω and D are angular frequency and noise intensity for forcing currents; $Q(t)$ is phase noise; and I_{Na}, I_K, and I_{Leak} are sodium ion current, potassium ion current, and leakage current. Their expressions are as follows:

$$\begin{aligned} I_{Na} &= g_{Na} m_\infty(V)(1-n)(V - E_{Na}), \\ I_K &= g_K n (V - E_K), \\ I_{Leak} &= g_L (V - E_L), \\ I_D &= A\sin(Q(t)), \end{aligned}$$

where the parameter g_{Na} and g_K are the maximal conductances (mS/cm^2); E_{Na}, E_K, and E_L are the reversal potentials (mV); m_∞ and n_∞ are the steady-state of the ionic gating channels; and A is amplitude for forcing currents. They are modeled using:

$$m_\infty(V) = \frac{1}{1 + exp\left(-\frac{V+35}{5}\right)}, n_\infty(V) = \frac{1}{1 + exp\left(-\frac{V+36}{5}\right)}.$$

Specifically, we add a voltage-dependent linear control current (I) to this model, which is expressed as follows.

$$\frac{dI}{dt} = \varepsilon(-80 - V). \tag{2.2}$$

Now, ε is the feedback coefficient, and $\varepsilon = 0.001$ is used if not otherwise specified.

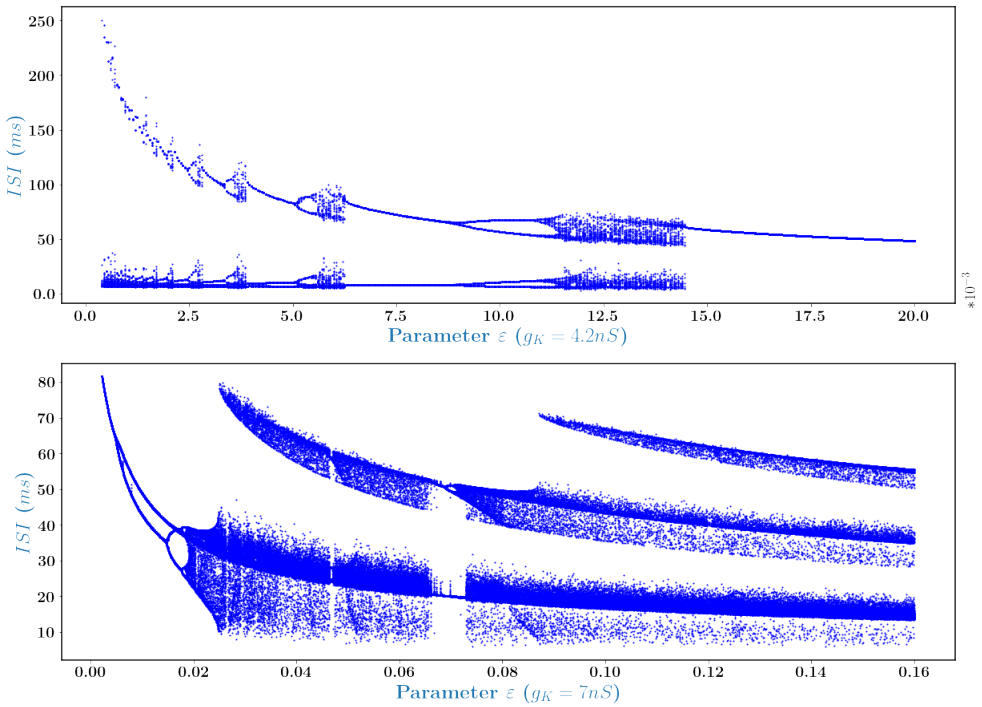

Figure 1. Sequence diagram of interspike intervals of a single neuron for $g_K = 4.2nS$ and $7nS$, as the change of parameter ε.

By adjusting parameters, the HH model can reproduce the firing patterns observed in neurons, which underlie their rhythmic properties in the CPG. Figure 1 displays the sequence diagram of interspike intervals (ISIs) of a single neuron without noise. When $g_K = 4.2nS$, the system undergoes period-doubling bifurcation with the change of parameter ε, leading to chaos. At this point, the system has two period-doubling cascade paths, and the range of parameters that produce chaos broadens as ε increases. One period-doubling cascade path disappears around $\varepsilon = 0.0145$, while the other path has an interspike interval remaining. As we will see below, the system displays the spiking mode when $\varepsilon > 0.0145$. When $g_K = 7nS$, the system shows a bifurcation diagram that resembles the period-adding cascade as parameters increase. There is still a bifurcation path from period-doubling to chaos. The ISI diagram clearly shows three layers, which may contain deep neural information not captured by the firing patterns of neurons. In the following section, we will present the firing sequence diagram for the corresponding parameters of Figure 1.

In Figure 2, the left panel displays the time series for $g_K = 4.2nS$ (above Figure 1). When $\varepsilon = 0.001$, the neuron model exhibits bursting, which corresponds to several ISIs shown in Figure 1. For $\varepsilon = 0.005$ and 0.0075, there are three and two ISIs respectively, represented by three spikings and two spikings per bursting. When $\varepsilon = 0.01$, this extends to four ISIs, and although the firing pattern appears similar to that of $\varepsilon = 0.0075$, it has changed. At $\varepsilon = 0.0125$, the system discharges chaotically, while at $\varepsilon = 0.015$, the firing is a single spiking. The right panel of Figure 2 displays the time series for $g_K = 7nS$ (below Figure 1). At $\varepsilon = 0.01$, the model discharge shows two ISIs. As the parameter varies from 0.02 to 0.014, the discharge pattern of the model exhibits different chaotic discharges. In this manner, by calculating the ISIs, we can observe the hidden information of the firing sequence.

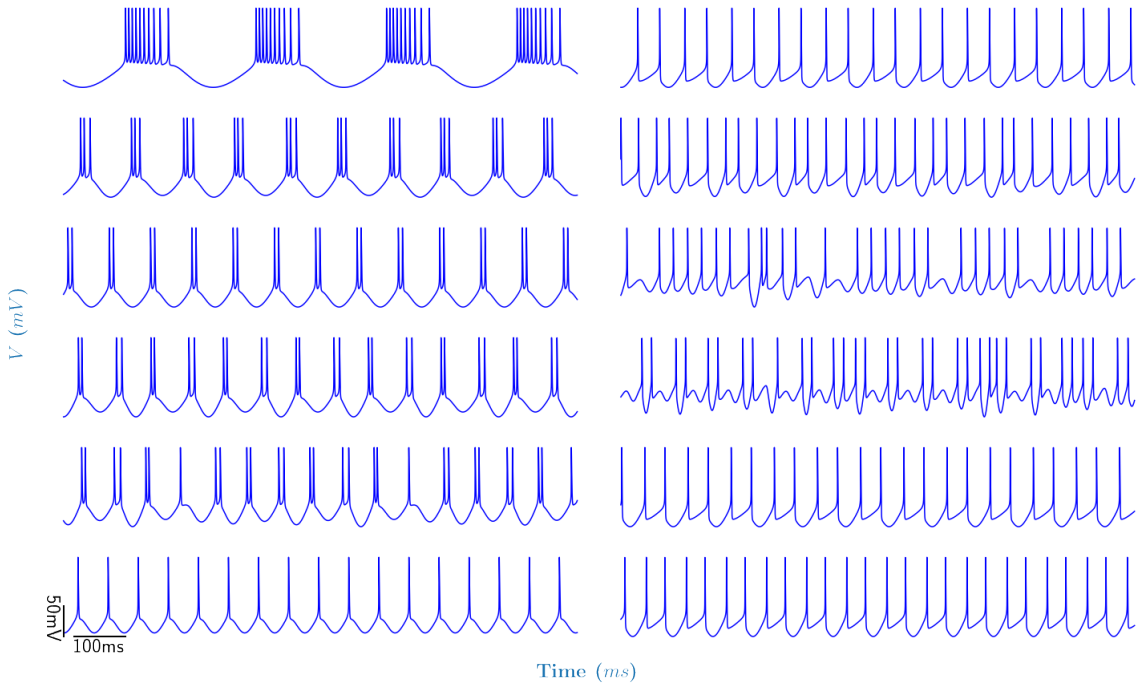

Figure 2. Time series diagram. Left panel $g_K = 4.2nS$ and parameter ε from top to bottom is 0.001, 0.005, 0.0075, 0.01, 0.0125, 0.015; right panel $g_K = 7nS$ and parameter ε from top to bottom is 0.01, 0.02, 0.04, 0.08, 0.12, 0.14.

2.2. CPG based model

The inhibitory relationship between neurons is considered to be a key point in the generation of rhythms. Our CPG models typically consist of two or three neurons. The most common structure describing firing rhythmic activities consists of two coupled neurons that inhibit each other (Figure 3A). This structure is widely known as half-center oscillator and is symmetrically coupled through both inhibitory connections with g_{12} and g_{21}. We will start off with the simplest network where two cells next section. On this basis, we extended the number of neurons to three (Figure 3B,C). In three circuits, neurons and inhibitory synapses (small black solid dots) form a hybrid microcircuit. And neurons are labeled with different colors (blue, red and green) which correspond to the colors in the firing activities. The synaptic transmission contained in the CPG structure in Figure 3 are ionotropic synapses. These synaptic are inhibitory synapses and are modeled using a first-order kinetic equations, which are conductance-based type similar to previous studies [48–51]:

$$\begin{cases} I_{pre\to post} &= g_{pre\to post} H_\infty(V_{pre})\left(V_{pre} - E_{pre\to post}\right), \\ H_\infty(V_{pre}) &= \dfrac{1}{1 + exp\left(-\dfrac{V_{pre} - \theta}{\sigma}\right)}. \end{cases} \tag{2.3}$$

Here, V_{pre} is the presynaptic voltage, $\sigma = 1mV$ is the steepness, $\theta = -60mV$ sets the value when the function is semi-activated, $E_{pre\to post}$ is the reversal potential, and $g_{pre\to post}$ is the maximal conductance (g_{ij}, $i, j = 1, 2, 3$ & $i \neq j$ in Figure 3).

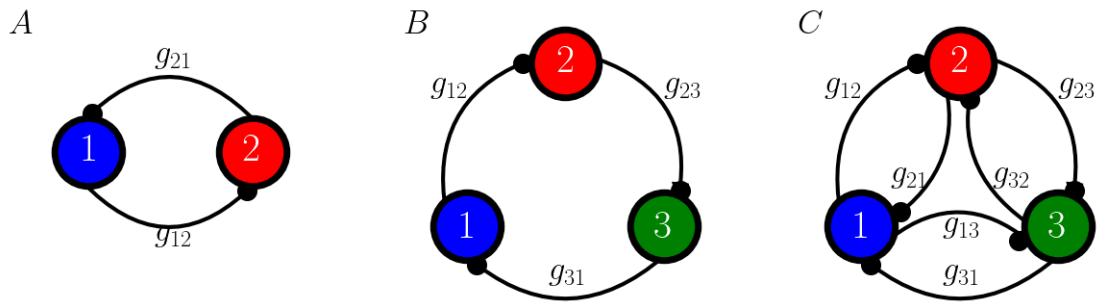

Figure 3. Three different topologies of mutually inhibited neuronalcircuits in this study. The solid blue, green, and red circles represent neurons and are labeled as 1, 2 and 3, respectively. These neurons are modeled by the HH model, see eqs 2.1 and 2.2. Black filled circles represent inhibitory synapses and the model see eq 2.3. The conductance of the connection between neurons is noted as g_{ij}, $i, j = 1, 2, 3$ & $i \neq j$. This indicates that the synapse from neuron i to neuron j.

For numerical integration of network system, the fourth-order Runge–Kutta algorithm was used with a time step of $0.05ms$. The total integration time length of each simulation run was $5000ms$. Simulations were implemented in Python 3.9.7 on PC with $12th$ Gen Intel(R) Core(TM) i7-12700H 2.30 GHz CPU.

3. Results

3.1. The rhythm activity of half-center oscillator

The discussion in this section is based on the reciprocal inhibition of two neurons, which we call half-center oscillators (pattern A in Figure 3). The synchronous firing of neurons contains very important neural information. Here we investigate the synchrony of half-central oscillator rhythm activity. In Figure 4, we show the variation trend of synchronous firing with synaptic parameters of the model, and we can see the roughly synchronous discharge pattern. Fixing the synaptic parameter σ, we can find that the reversal potential E_{syn} has an intermittent effect on synchrony. The effect of the synaptic parameter σ is more continuous than fixing it. The transversely separated bands are very distinct, indicating that the synaptic reversal potential has a significant effect on synchrony. In the following, we will select three appropriate sets of parameters to investigate the synchronization of half-central oscillation according to the phase difference diagram shown in Figure 4. The three sets of parameters are $E_{syn} = -110mV$, $\sigma = 1$ (phase difference between $100ms$ and $200ms$); $E_{syn} = -89mV$, $\sigma = 1/2$ (phase difference between 200 and $250ms$); and $E_{syn} = -61mV$, $\sigma = 1/6$ (phase difference between 0 and $50ms$).

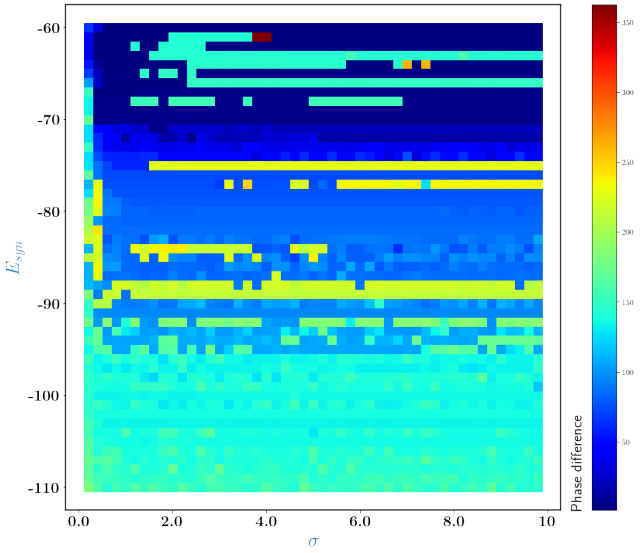

Figure 4. The phase difference bifurcation diagram of the model firing under the change of the bissynaptic parameters. σ and E_{syn} are two synaptic parameters. The smaller the value of the phase difference, the closer it is to synchronization.

From the top of the Figure 5 (i.e., when the synaptic parameters are $E_{syn} = -110mV$ and $\sigma = 1$), as the two-parameter synaptic conductance is changed, the phase difference of the neuronal membrane potential exceeds 100 except near the diagonal. The diagonal is shown in dark blue, indicating that the two neurons are perfectly synchronized. By simulating their discharge state, it can also be confirmed that synchronization is achieved when the conductance parameters of the two synapses are equal. In particular, in the small regime of two synaptic conductances close to zero and close to one, the area of perfect synchrony is slightly larger. Dark purple indicates that the phase difference between the two neurons is maximal. One interesting observation is that the bifurcation diagram of the phase difference is symmetric about the diagonal as the two-parameter synaptic conductance change.

When the synaptic parameters were changed to $E_{syn} = -89mV$ and $\sigma = 1/2$, we obtained the synchronous firing diagram of the half-center oscillator as shown in the middle of Figure 5. The diagonal synchrony seems to be preserved as we can see from the figure. However, the discharge of the diagonal is richer (The variety of the phase difference indicates the richness in the rhythm activity of the half-central oscillator). The bifurcation diagram of the phase difference is still symmetric and we can get a variety of differences in the phase difference depending on the color distribution of the pattern. A variety of rhythm activities of the half-center oscillator can be realized, which makes it easier to operate and transform the half-center oscillator. Furthermore, we can perform the rhythm control of the half-center oscillator. Eventually, we may be able to achieve synchronous control of a half-central oscillator. Synchronization does not necessarily require the two-parameter synaptic conductance to be equal as can be seen from the bottom of Figure 5. Unlike in the previous two diagrams, the distinct dark blue diagonals are missing, but the symmetry about the synaptic conductance is preserved. Here the dark blue area is spread throughout the parameter bifurcation plane and the phase difference is radially spread around the upper right corner, like a ripple of water. Based on the above analysis, small synaptic conductance parameters may make it easier to achieve the synchronous rhythm of the half-center oscillator, and synaptic parameters E_{syn} and σ have significant effects on their synchronization.

In the following, we will investigate the ISIs of each neuron in the half-center oscillator model with different potassium conductance g_K under the above three sets of parameters. The left panel of Figure 6 depicts the bifurcation diagram under the three groups of parameters when the conductance parameter is $4.2nS$. It can be seen from the figure that the rhythm activity in the half-center oscillator of the three bifurcation graphs is not synchronous. The top is like a bifurcation process of inverse period-adding and the discharge of the system is relatively stable. We can see that the discharge is very abundant from the middle, especially when the ε is between 0.01 and 0.015, which can be related to the middle of Figure 5. The bottom shows the complex diversity of ISIs. Like the first two, ISIs are concentrated in two layers and it is in a chaotic state. This corresponds to the bottom of Figure 5 and it is interspersed with large phase differences dotted with dots. When the potassium conductance $g_K = 7nS$, the ISIs for the three sets of parameters are shown on the right panel of Figure 6. Compared with the left panel, the ISIs have changed fundamentally. Neuron 1 in the half-center oscillator shows smaller ISIs than neuron 2 shown at the top. In the middle, there is only one ISI in the former stage, and the chaotic ISIs start to appear in the later stage. Therefore, the change in potassium conductance has a great influence on the rhythm activity of the half-center oscillator.

We analyzed the bifurcation patterns and the ISIs patterns of the half-center oscillator to investigate the rhythm activity when the potassium conductance is changed. Our research found that altering the relative size of the two-parameter synaptic conductances could control the rhythm pattern of the half-center oscillator. Different synaptic parameters such as E_{syn} and σ can trigger very different rhythm patterns. Figure 7 presents an example where we took $E_{syn} = -110mV$, $\sigma = 1$, $g_{12} = 0.2nS$, $g_{21} = 0.8nS$ to investigate the HCO rhythm under different potassium conductances. It turns out that a single spike on the left panel has branches that cause neuron 1's ISIs to decrease when noise is added to it. We looked at the bursts rhythm, spiking rhythm, and mixed mode rhythm in HCO. A large number of discharge patterns can be implemented in HCO, especially when $g_K = 7nS$, by adjusting the asymmetric coupling factor. By comparing the rhythmic activity, we found that when g_{12} is larger than g_{21}, neuron 1 fires earlier than neuron 2, and vice versa. In other words, synaptic conductance parameters can control the firing start time of neurons in HCO. Synapse conductance parameters can also synchronize discharge patterns in HCO as shown in Figure 8 under different discharge modes when the synaptic parameters are exactly equal. Different discharge mode synchronization will occur under different conductances such as burst synchronization, spiking synchronization, and subthreshold synchronization. We found that in HCO, the synchronization regime is likely to appear when the synaptic conductance parameters are equal, but the synchronization state will also appear when the synaptic conductance parameters are not equal. Synaptic parameters are required to participate in the mediation of neuron firing in this case. The inequality of the two synaptic parameters will lead to a rich rhythm pattern of HCO. The synchronization state disappears when noise acts on neuron 1. When $g_K = 4.2nS$, the rhythmic discharge of neuron 1 changes greatly, while the burster structure of neuron 2 is stable. When $g_K = 7nS$, the spiking of neurons is disturbed. In particular, when $g_K = 47.4nS$, only neuron 1, which was originally subthreshold began to discharge, while neuron 2 remained subthreshold.

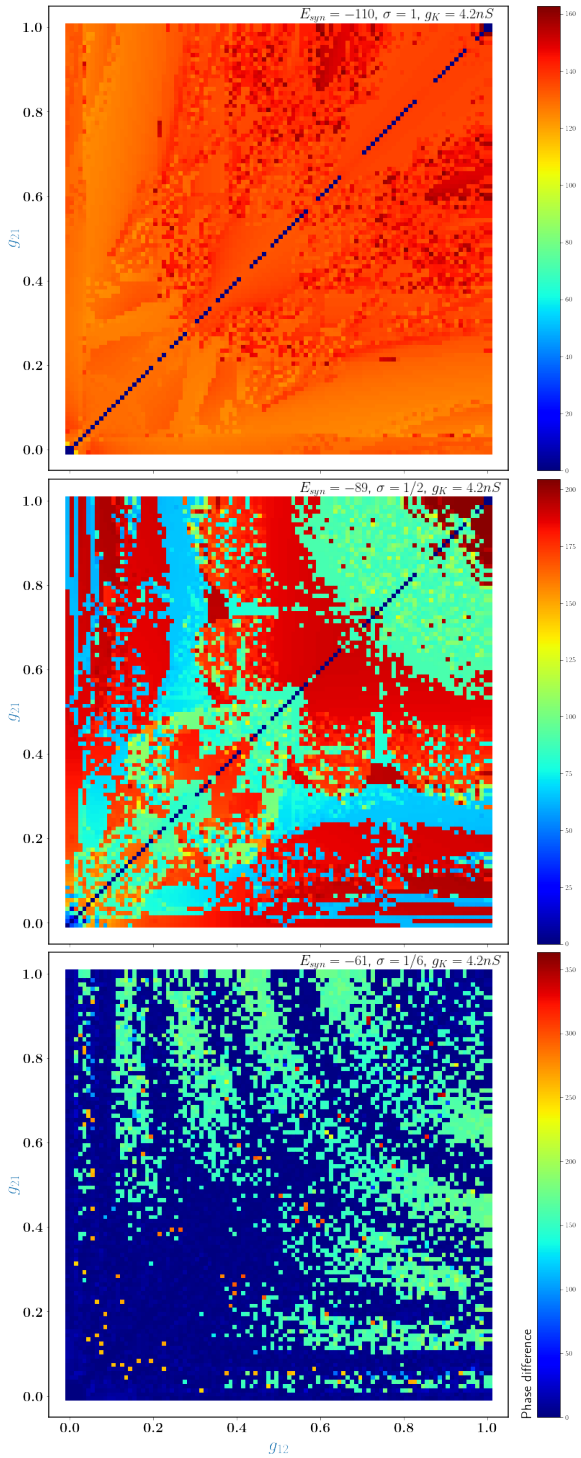

Figure 5. Phase bifurcation diagram as a function of asymmetric coupling factor. Synaptic parameters: top ($E_{syn} = -110$, $\sigma = 1$), middle ($E_{syn} = -89mV$, $\sigma = 1/2$), bottom ($E_{syn} = -61mV$, $\sigma = 1/6$). Potassium conductance $g_K = 4.2nS$. Here dark blue indicates gradual synchronization, and dark purple is the largest phase difference.

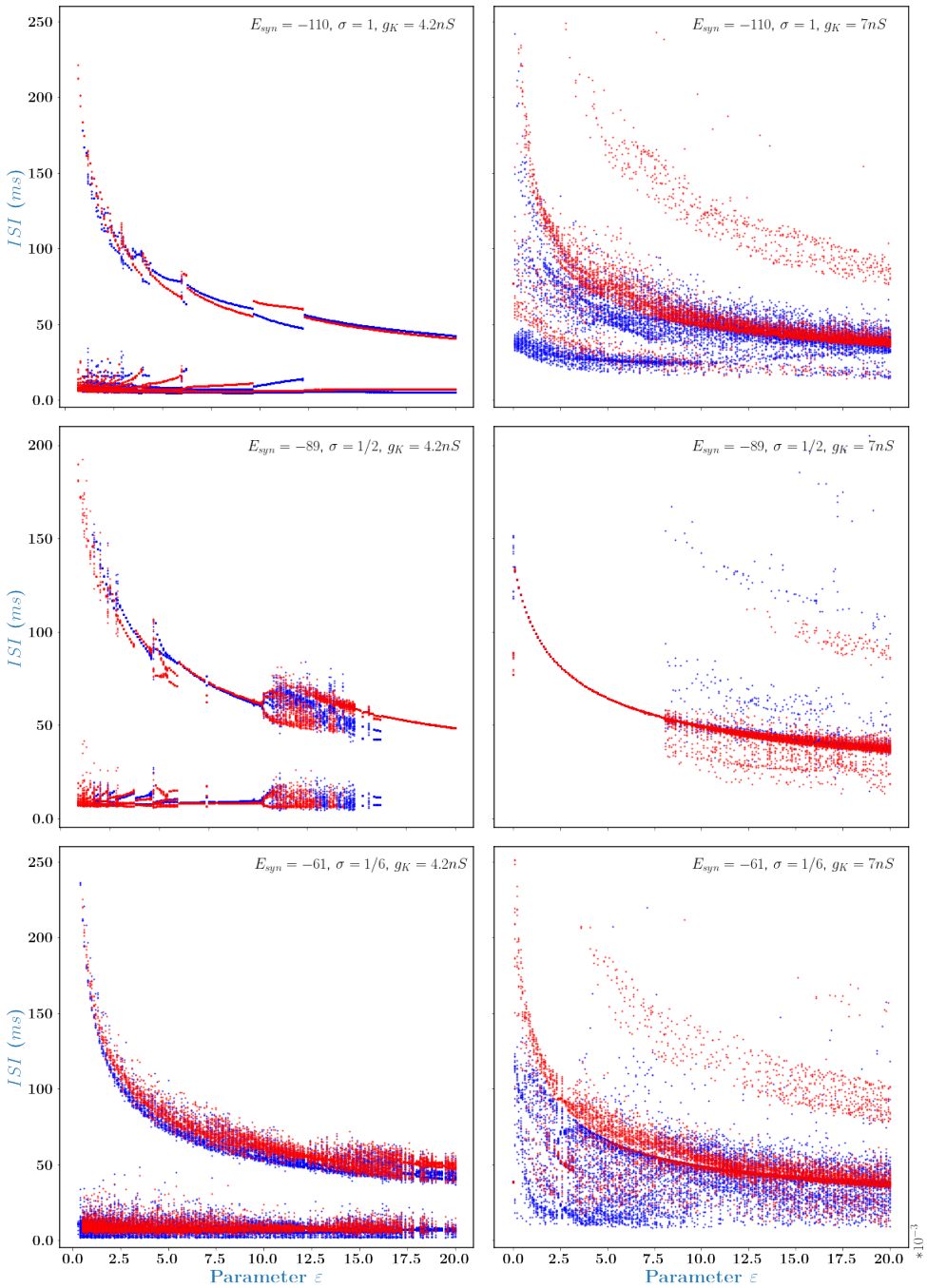

Figure 6. Sequence diagram of interspike intervals of half-center oscillators. The blue track shows the ISIs of neuron 1, and the red track shows the ISIs of neuron 2. Synaptic parameters: top ($E_{syn} = -110mV$, $\sigma = 1$), middle ($E_{syn} = -89mV$, $\sigma = 1/2$), and bottom ($E_{syn} = -61mV$, $\sigma = 1/6$). Left panel: potassium conductance $g_K = 4.2nS$; right panel: potassium conductance $g_K = 7nS$.

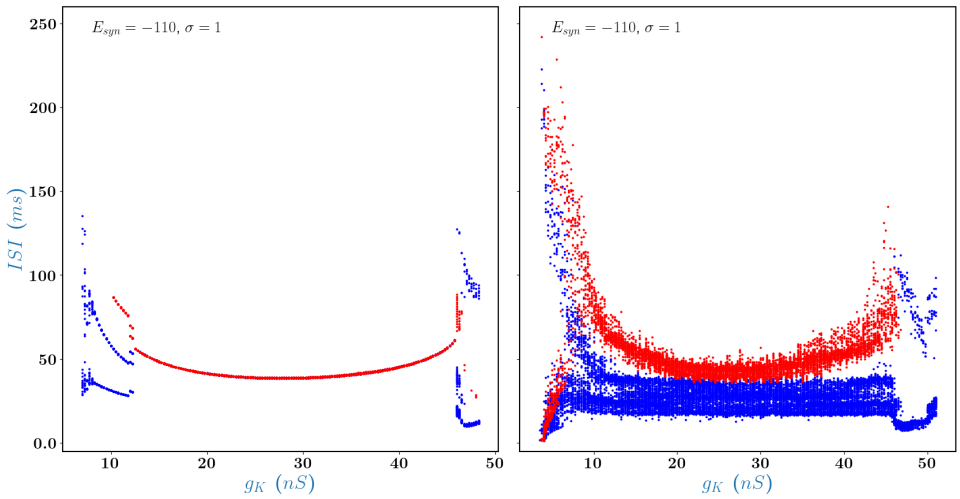

Figure 7. Sequence diagram of interspike intervals of half-center oscillators as potassium conductance changes. Blue shows the firing sequence of neuron 1, red shows the firing sequence of neuron 2. Synaptic conductance $g_{12} = 0.2nS$, $g_{21} = 0.8nS$. The left panel: HCO without noise, and the right panel: HCO with noise and parameters $A = 5, D = 2, \omega = 0.5$. Here the noise only acts on neuron 1.

Subthreshold oscillation contains rich expression of neuronal information [52]. Here, subthreshold oscillations of the half-center oscillator are shown in Figure 9. As you can be seen from the right panel, Subthreshold oscillations alternate between neurons 1 and 2 in HCO, and subthreshold oscillations appear accompanied by small oscillations at lower membrane voltage values. The subthreshold oscillations in neuron 2 are consistent with the current in synapse 2. A more detailed subthreshold oscillation process can be found in the left panel, where the membrane voltage value of neuron 2 hovers near the lowest center when subthreshold oscillation of neuron 1 begins. When neuron 1 ends subthreshold oscillation, it continuously changes to hover around smaller membrane voltage values, while neuron 2 begins subthreshold oscillation. This is how subthreshold oscillations of neurons 1 and 2 alternate.

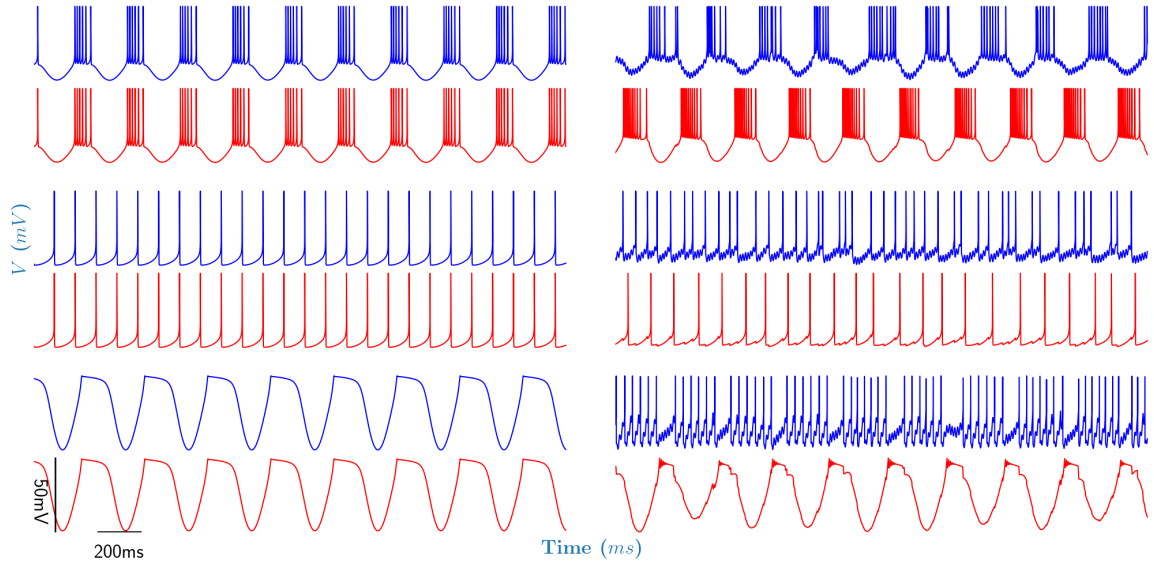

Figure 8. Synchronization of half-center oscillators rhythm activity. Synaptic conductance $g_{12} = 0.1nS$, $g_{21} = 0.1nS$. The top, middle, and bottom represent the synchronization of bursts mode, spiking, and subthreshold oscillation when $g_K = 4.2nS, 7nS$, and $47.4nS$, respectively. The left panel: HCO without noise, and the right panel: HCO with noise and parameters $A = 5, D = 2, \omega = 0.5$. Here the noise only acts on neuron 1.

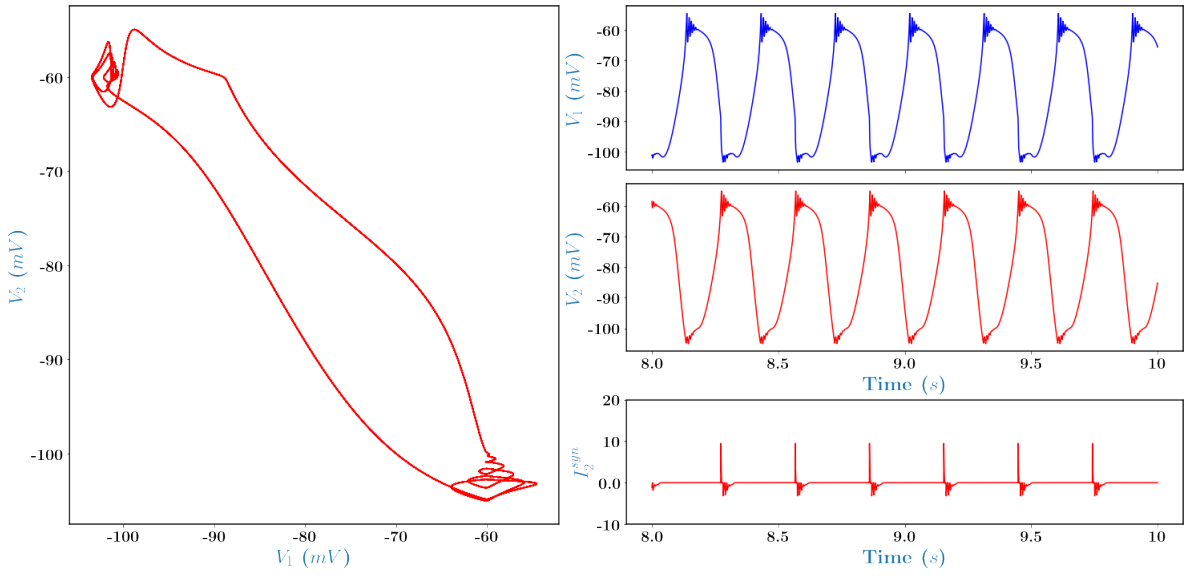

Figure 9. Subthreshold firing phase diagram of half-center oscillator. The left panel is the phase diagram. The right panel, from top to bottom, are the firing of neuron 1, firing of neuron 2, and the current at synapse 2. $g_K = 46.4nS$, $g_{12} = 0.5nS$, $g_{21} = 1.0nS$, $\sigma = 1/5$, $E_{syn} = -100mV$.

3.2. *Sequentially inhibit the connected CPG rhythm pattern*

This section discusses the patterns B and C (Figure 3) in a tri-neuron CPG. The time difference in calculating its discharge sequence is significant by comparing the single neuron, half-center oscillator, and tri-neuron CPG. The increase in the number of neurons will greatly reduce the computational efficiency. In contrast, the increase in the number of synapses will also affect the computational efficiency, but it is not as obvious as the increase in the number of neurons. Figures 10 and 11 show the discharge pattern in pattern B (Figure 3) under two different synaptic conductance parameters while fixing the potassium conductance $g_K = 4.2nS$ and two synaptic parameters $E_{syn} = -110mV$, $\sigma = 1$. Pattern B (Figure 3) is the sequential inhibition of connected neuronal circuits, g_{ij} indicates the synaptic conductance that the ith neuron inhibits the jth neuron.

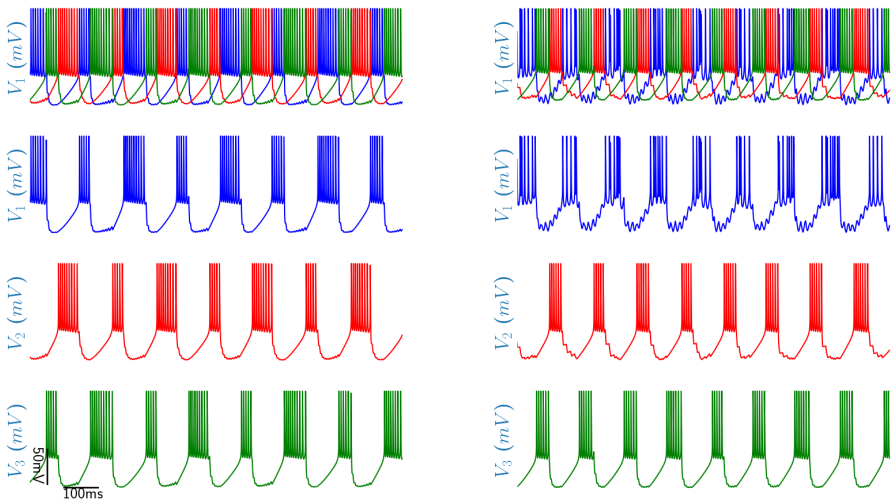

Figure 10. The rhythm pattern is in the tri-neuron CPG. Blue, red, and green are the membrane voltages of neurons 1–3, respectively. The synaptic conductance parameters are $g_{12} = 0.4nS$, $g_{23} = 0.6nS$, $g_{31} = 0.8nS$. The corresponding display is pattern B (Figure 3). The left panel: HCO without noise, and the right panel: HCO with noise and parameters $A = 5, D = 2, \omega = 0.5$. Here the noise only acts on neuron 1.

As can be seen from Figure 10, for this set of synaptic conductance parameters, members of CPG exhibit different rhythm patterns than those in single neurons and half-center oscillators, which are caused by synaptic coupling of neurons (left panel). If the discharge of blue neuron 1 is taken as the starting point of the member in CPG, the typical CPG rhythm pattern is shown, that is, the discharge order in CPG members is "blue-green-red" or "neuron 1-neuron 3-neuron 2". When the noise is applied to neuron 1, we find that the firing of neuron 1 changes greatly and the firing of neurons 2 and 3 changes weakly.

When we change the synaptic conductance $g_{12} = 0.1nS$ in Figure 10, the rhythm pattern shown in Figure 11 is obtained. At this time, the subtle shift in the discharge of members in CPG can be controlled by adjusting the synaptic conductance g_{12}. That is, the rhythm pattern control of such CPG members can be realized and changes in synaptic conductance regulate the rhythm pattern of members in CPG. When the noise is applied to neuron 1, the firing of neurons 2 and 3 changes weakly.

When the conductance of three synapses is equal, the members in CPG exhibit the same burst dis-

charge in pattern B (Figure 3). In pattern B, we found a small rule that increased synaptic conductance delayed the start time of postsynaptic neuron firing. When g_{31} is much smaller than g_{12}, neurons 3 and 1 tend to be in sync. Using this property, the firing synchronization of neurons in CPG can be easily regulated and controlled.

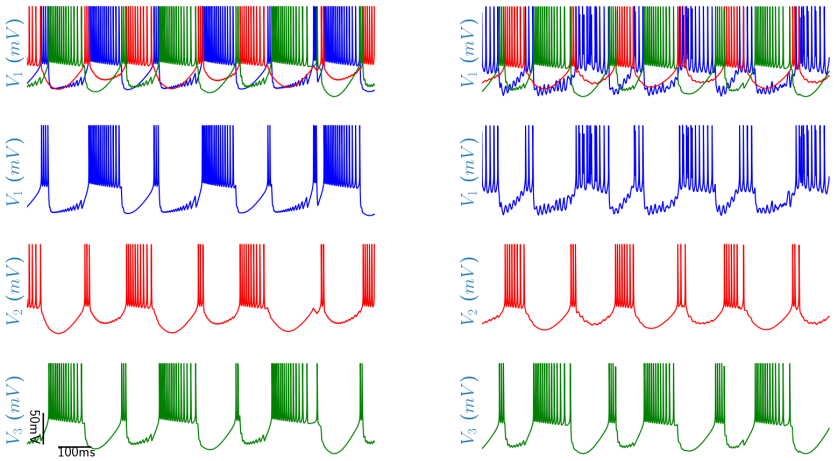

Figure 11. The rhythm pattern is in the tri-neuron CPG. Blue, red, and green are the membrane voltages of neurons 1–3, respectively. The synaptic conductance parameters are $g_{12} = 0.1nS$, $g_{23} = 0.6nS$, $g_{31} = 0.8nS$. The corresponding display is pattern B (Figure 3). The left panel: HCO without noise, and the right panel: HCO with noise and parameters $A = 5, D = 2, \omega = 0.5$. Here the noise only acts on neuron 1.

3.3. CPG rhythm patterns of reciprocal inhibition connections

In the same way, we also analyze the rhythm pattern of tri-neuron CPG, namely pattern C (Figure 3). This pattern is a tri-neuron circuit composed of pairs of neurons that inhibit each other. Although it has the same two discharge sequences as the members of CPG in pattern B (Figure 3), the discharge mode of members in CPG is completely different from that of pattern B (Figure 3), as shown in Figure 12. At this time, the discharge order of CPG members showed "neuron 1-neuron 2-neuron 3", but the membrane voltage sequence of neuron 1 is different from that of neurons 2 and 3. Unlike the Figure 10, each member of the CPG behaves in the same discharge. That is, the reciprocal inhibition of the CPG loop increases the diversity of the discharge activities of its members. In addition, we found that when noise was stimulated to neurons 1–3 respectively, the stimulation of neuron 2 completely destroyed the original CPG firing rhythm pattern. The reason may be that the synaptic conductance parameters of neuron 2 are very small.

In particular, when the conductance of each synapse in the CPG is different (As shown in Figure 13), the member of CPG named neuron 1 shows an burster firing pattern, while neurons 2 and 3 show a mixed bursting pattern. The discharge activities of such CPG members are caused by completely asymmetric coupling factor regulation. The results show that asymmetric coupling factors can strongly regulate the discharge of neurons. Under these synaptic parameters, the firing rhythm pattern was substantially altered when we stimulated neurons 1–3 with noise, respectively. This may be because CPG at this synaptic parameter is in a critical state. The members of CPG show very rich discharge activities in pattern C (Figure 3), not all of which are shown here. We also investigated the patterns of

two other types of synaptic connections in which members also have different discharges, only two of which are shown here.

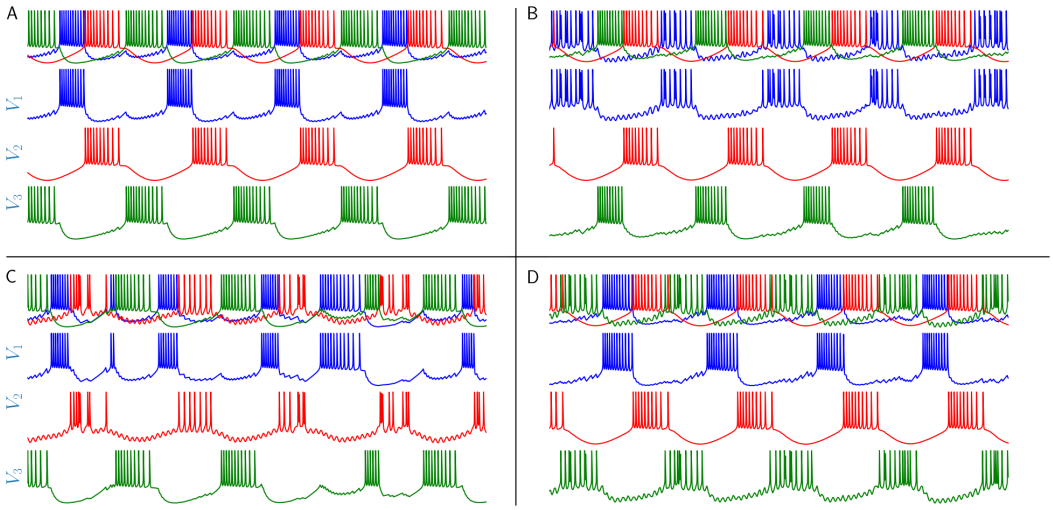

Figure 12. The rhythm pattern is in the tri-neuron CPG. Blue, red, and green are the membrane voltages of neurons 1–3, respectively. The synaptic conductance parameters are $g_{12} = 0.02nS$, $g_{23} = 0.2nS$, $g_{31} = 0.3nS$, $g_{21} = 0.3nS$, $g_{32} = 0.02nS$, $g_{13} = 0.2nS$. The corresponding display is pattern C (Figure 3). A) represents HCO without noise; B), C) and D) represent HCO with noise and parameters $A = 5, D = 2, \omega = 0.5$. Here the noise only acts on neuron 1 (B), neuron 2 (C), and neuron 3 (D), respectively.

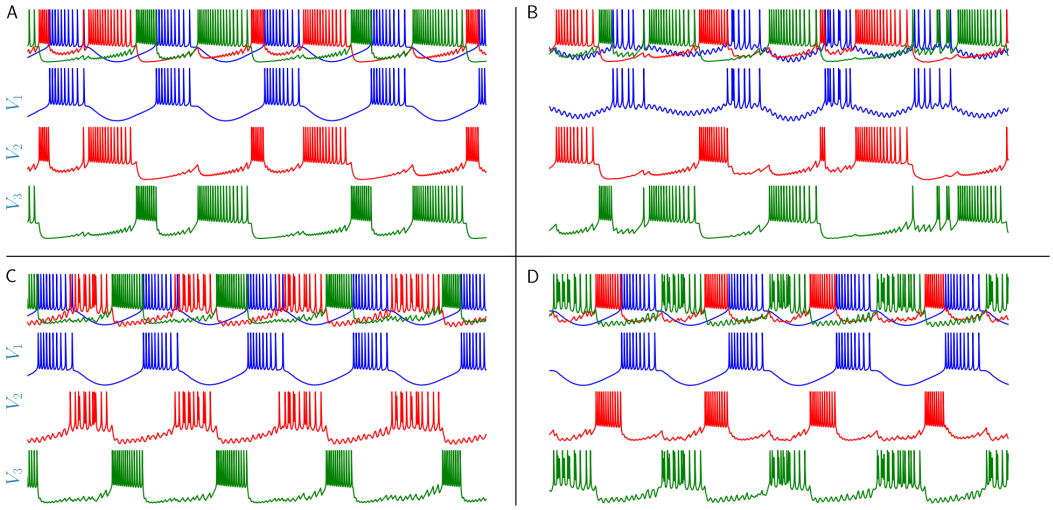

Figure 13. The rhythm pattern is in the tri-neuron CPG. Blue, red, and green are the membrane voltages of neurons 1–3, respectively. The synaptic conductance parameters are $g_{12} = 0.3nS$, $g_{23} = 0.5nS$, $g_{31} = 0.02nS$, $g_{21} = 0.02nS$, $g_{32} = 0.4nS$, $g_{13} = 0.6nS$. The corresponding display is pattern C (Figure 3). A) represents HCO without noise; B), C) and D) represent HCO with noise and parameters $A = 5, D = 2, \omega = 0.5$. Here the noise only acts on neuron 1 (B), neuron 2 (C), and neuron 3 (D), respectively.

4. Conclusions

This paper first introduces the rich discharge properties of the single neuron model, which has been used in our modeling. Second, the influence of asymmetric coupling factor and two synaptic parameters σ and E_{syn} on the half-center oscillators discharge synchronization is discussed. We find that synaptic parameters and noise together affect the discharge of two neurons in the half-center oscillator. Asymmetric coupling factors modulate the rhythm activity in the half-center oscillator. We find that the firing synchronization occurred not only at the diagonal, but also when the remaining two synaptic parameters σ and E_{syn} are changed. Small synaptic conductance parameters may make it easier to synchronize the half-center oscillator, and the synaptic conductance may control the discharge order of neurons in the half-center oscillator. The interspike intervals diagram of two neurons in the half-center oscillator is used to verify the firing synchronization under several fixed parameters. In addition to the synaptic conductance parameters, the synaptic parameters σ and E_{syn} can be adjusted to increase the diversity of rhythm activity of the half-center oscillator. The synaptic conductance and synaptic parameters together control its rhythm activities. The rhythms properties of CPG are regulated by the potassium conductance value. The typical CPG modes and discharge synchronization of three groups of different potassium conductance parameters are shown, which are bursting, spiking, and mixed-mode oscillations (MMOs) respectively. It has been shown that noise can regulate the discharge rhythm and synchronization of HCO. Finally, two typical pattern are discussed, and how the asymmetric coupling factors regulate the discharge of members in CPG is analyzed.

The asymmetric coupling factor can adjust the discharge mode of CPG members, such as bursting mode, spiking, and MMOs, to realize the control of rhythms activity in CPG. The phase diagram explains the alternations between neuronal firing patterns and the effect of synaptic currents on membrane potential. We simulated six connected modes, and only the discharge modes of members in partial CPG of the three types were shown here. We find that the rhythm activity of neurons in patterns B and C (Figure 3) were more abundant than those in single and half-center oscillators neurons. Asymmetric coupling factors (synaptic conductance) can control the start time of postsynaptic neuron firing, and the increase of synaptic conductance will delay the start time of postsynaptic neuron firing. When potassium conductance g_K is changed, the discharge of CPG members will be greatly changed. For example, when $g_K = 7nS$, the members of CPG show abundant spiking discharge mode in pattern B (Figure 3). In the reciprocal inhibition CPG pattern C (Figure 3), when the potassium conductance $g_K = 4.2nS$ and the synaptic conductance is equal, the members of CPG do not discharge synchronously, which is different from the performance of pattern B (Figure 3). When the potassium conductance $g_K = 7nS$ and the synaptic conductance is equal, the discharge of the CPG members does not spiking synchronously, which is a very interesting question but we have not shown the diagram in detail here due to space constraints. That will be one of the things we will look at in the future. In addition, we found that noise and synaptic strength together determine the robustness of CPG, and the critical state of CPG rhythmic discharge is sensitive to noise. Furthermore, we have observed the same noise had a greater effect on the rhythm changes of neurons with lower synaptic strength. That is, high strength inhibition connection will improve the stability of CPG. Of course, the changes in synaptic parameters can also regulate the discharge mode of CPG members, so these factors will jointly determine the discharge mode of CPG members. The influence of comprehensive factors will be the focus and difficulty of our future research, and the rhythm activities of other members will also need to be

investigated. Finally, synapse parameters will be integrated to control and realize the rhythm activity of CPG.

Our study focused on the chemical synapses between neurons, while the electrical coupling between them was not considered. However, in future studies, we will analyze the synergistic effects of both electrical and chemical coupling in CPG as it can lead to very different rhythmic patterns. Our current model demonstrates that synaptic conductance can influence the rhythm pattern of the tri-neuron network and a change in the conductance can shift the members of the CPG into typical regular sequential discharge mode. Our findings reveal a unique rhythm pattern in CPG, where neuron 1 exhibits chaotic spiking while neurons 2 and 3 show regular bursting. This rhythmic activity and regular sequential discharge pattern of the CPG is crucial for its flexibility, robustness, and ultimate realization of swimming, walking, or other cognitive functions. The diversity of rhythm activities in CPG is essential for its flexibility and robustness, which can resist interference from external information. Changes in synaptic conductance and noise can produce a large number of different rhythm activities, making the CPG less susceptible to external interference.

CPG rhythm patterns have been discovered in invertebrates (crustacean pyloric or gastric) and leech heartbeats. These patterns are used to simulate the rhythm activity of the human central nervous system, which in turn controls the rhythm of arm movement [17]. Additionally, CPG rhythm can help in the diagnosis of various diseases. For instance, Mader et al. [1] have claimed that CPG can assist in the development of therapeutic methods for the recovery of strong spinal cord injuries. Tassinari et al. reviewed the relationship of central pattern generators with parasomnias and sleep-related epileptic seizures and explained some epileptic seizures and parasomnias using the firing patterns of the CPG [53, 54]. Therefore, studying the functioning principle of CPG rhythm activities is essential for understanding related motor behaviors and achieving better motor control as well as improving disease diagnosis.

Use of AI tools declaration

The authors declare they have not used Artificial Intelligence (AI) tools in the creation of this article.

Acknowledgments

This work was funded by the National Natural Science Foundation of China (Grant Nos. 12202208 and 11872183), the Basic Science (Natural Science) Research Project of Colleges and Universities of Jiangsu Province (Grant No. 22KJB130009), the Research and Cultivation Project for Young Teachers of Nanjing Audit University (Grant No. 2021QNPY015), 2022 Doctoral program of Entrepreneurship and Innovation in Jiangsu Province (Grant No. JSSCBS20220717), the China Scholarship Council (Grant No. 202206150096).

Conflict of interest

The authors declare there is no conflict of interest.

References

1. E. Marder, D. Bucher, Central pattern generators and the control of rhythmic movements, *Curr. Biol.*, **11** (2001), R986–R996. https://doi.org/10.1016/S0960-9822(01)00581-4
2. E. Marder, R. L. Calabrese, Principles of rhythmic motor pattern generation, *Physiol. Rev.*, **76** (1996), 687–717. https://doi.org/10.1152/physrev.1996.76.3.687
3. A. Sakurai, C. A. Gunaratne, P. S. Katz, Two interconnected kernels of reciprocally inhibitory interneurons underlie alternating left-right swim motor pattern generation in the mollusk Melibe leonina, *J. Neurophysiol.*, **112** (2014), 1317–1328. https://doi.org/10.1152/jn.00261.2014
4. D. Alaçam, A. Shilnikov, Making a swim central pattern generator out of latent parabolic bursters, *Int. J. Bifurcation Chaos*, **25** (2015), 1540003. https://doi.org/10.1142/S0218127415400039
5. A. I. Selverston, *Model Neural Networks and Behavior*, New York, 1985. https://doi.org/10.1007/978-1-4757-5858-0
6. W. N. Frost, P. S. Katz, Single neuron control over a complex motor program, *PNAS*, **93** (1996), 422–426. https://doi.org/10.1073/pnas.93.1.422
7. P. S. Katz, S. L. Hooper, Invertebrate central pattern generators, *Cold Spring Harbor Monogr. Ser.*, **49** (2007), 251.
8. E. Marder, S. Kedia, E. O. Morozova, New insights from small rhythmic circuits, *Curr. Opin. Neurobiol.*, **76** (2022), 102610. https://doi.org/10.1016/j.conb.2022.102610
9. E. Marder, Neuromodulation of neuronal circuits: back to the future, *Neuron*, **76** (2012), 1–11. https://doi.org/10.1016/j.neuron.2012.09.010
10. I. Belykh, A. Shilnikov, When weak inhibition synchronizes strongly desynchronizing networks of bursting neurons, *Phys. Rev. Lett.*, **101** (2008), 078102. https://doi.org/10.1103/PhysRevLett.101.078102
11. T. Nowotny, M. I. Rabinovich, Dynamical origin of independent spiking and bursting activity in neural microcircuits, *Phys. Rev. Lett.*, **98** (2007), 128106. https://doi.org/10.1103/PhysRevLett.98.128106
12. A. I. Selverston, Invertebrate central pattern generator circuits, *Phil. Trans. R. Soc. B*, **365** (2010), 2329–2345. https://doi.org/10.1098/rstb.2009.0270
13. A. I. Selverston, M. I. Rabinovich, H. D Abarbanel, R. Elson, A. Szücs, R. D. Pinto, et al., Reliable circuits from irregular neurons: a dynamical approach to understanding central pattern generators, *J. Physiol.-Paris*, **94** (2000), 357–374. https://doi.org/10.1016/S0928-4257(00)01101-3
14. R. Huerta, M. A. Sánchez-Montañés, F. Corbacho, J. A. Sigüenza, A central pattern generator to control a pyloric-based system, *Biol. Cybern.*, **82** (2000), 85–94. https://doi.org/10.1007/PL00007963
15. M. Lodi, A. L. Shilnikov, M. Storace, Design principles for central pattern generators with preset rhythms, *IEEE Trans. Neural Networks Learn. Syst.*, **31** (2019), 3658–3669. https://doi.org/10.1109/TNNLS.2019.2945637
16. S. Chen, Y. Liu, T. Chen, J. Lou, Rhythm motion control in bio-inspired fishtail based on central pattern generator, *IET Cyber-Syst. Robot.*, **3** (2021), 53–67. https://doi.org/10.1049/csy2.12007

17. J. Wojcik, J. Schwabedal, R. Clewley, A. L. Shilnikov, Key bifurcations of bursting polyrhythms in 3-cell central pattern generators, *PLoS One*, **9** (2014), e92918. https://doi.org/10.1371/journal.pone.0092918

18. J. T. C. Schwabedal, A. B. Neiman, A. L. Shilnikov, Robust design of polyrhythmic neural circuits, *Phys. Rev. E*, **90** (2014), 022715. https://doi.org/10.1103/PhysRevE.90.022715

19. R. Azodi-Avval, F. Bahrami, A mathematical model of arm movement during rhythmic motor activity, in *2011 18th Iranian Conference of Biomedical Engineering (ICBME)*, (2011), 304–308. https://doi.org/10.1109/ICBME.2011.6168578

20. M. B. Reyes, P. V. Carelli, J. C. Sartorelli, R. D. Pinto, A modeling approach on why simple central pattern generators are built of irregular neurons, *PLoS One*, **10** (2015), e0120314. https://doi.org/10.1371/journal.pone.0120314

21. J. Dethier, G. Drion, A. Franci, R. Sepulchre, A positive feedback at the cellular level promotes robustness and modulation at the circuit level, *J. Neurophysiol.*, **114** (2015), 2472–2484. https://doi.org/10.1152/jn.00471.2015

22. J. Collens, K. Pusuluri, A. Kelley, D. Knapper, T. Xing, S. Basodi, et al., Dynamics and bifurcations in multistable 3-cell neural networks, *Chaos*, **30** (2020), 072101. https://doi.org/10.1063/5.0011374

23. Q. Lu, X. Wang, J. Tian, A new biological central pattern generator model and its relationship with the motor units, *Cognit. Neurodyn.*, **16** (2022), 135–147. https://doi.org/10.1007/s11571-021-09710-0

24. Q. Lu, J. Tian, Synchronization and stochastic resonance of the small-world neural network based on the CPG, *Cognit. Neurodyn.*, **8** (2014), 217–226. https://doi.org/10.1007/s11571-013-9275-8

25. Y. Zang, E. Marder, Neuronal morphology enhances robustness to perturbations of channel densities, *PNAS*, **120** (2023), e2219049120. https://doi.org/10.1073/pnas.2219049120

26. E. M. Izhikevich, Neural excitability, spiking, and bursting, *Int. J. Bifurcation Chaos*, **10** (2000), 1171–1266. https://doi.org/10.1142/S0218127400000840

27. B. Lu, X. Jiang, Reduced and bifurcation analysis of intrinsically bursting neuron model, *Electron. Res. Arch.*, **31** (2023), 5928–5945. https://doi.org/10.3934/era.2023301

28. F. Zhan, S. Liu, X. Zhang, J. Wang, B. Lu, Mixed-mode oscillations and bifurcation analysis in a pituitary model, *Nonlinear Dyn.*, **94** (2018), 807–826. https://doi.org/10.1007/s11071-018-4395-7

29. W. B. Kristan, Neuronal decision-making circuits, *Curr. Biol.*, **18** (2008), R928–R932. https://doi.org/10.1016/j.cub.2008.07.081

30. K. L. Briggman, W. B. Kristan, Multifunctional pattern-generating circuits, *Annu. Rev. Neurosci.*, **31** (2008), 271–294. https://doi.org/10.1146/annurev.neuro.31.060407.125552

31. A. A. A. Hill, J. Lu, M. A. Masino, O. H. Olsen, R. L. Calabrese, A model of a segmental oscillator in the leech heartbeat neuronal network, *J. Comput. Neurosci.*, **10** (2001), 281–302. https://doi.org/10.1023/A:1011216131638

32. R. L. Calabrese, Half-center oscillators underlying rhythmic movements, in *The Handbook of Brain Theory and Neural Networks*, (1998), 444–447.

33. Y. Zang, S. Hong, E. D. Schutter, Firing rate-dependent phase responses of Purkinje cells support transient oscillations, *eLife*, **9** (2020), e60692. https://doi.org/10.7554/eLife.60692

34. M. Liu, L. Duan, In-phase and anti-phase spikes synchronization within mixed Bursters of the pre-Bözinger complex, *Electron. Res. Arch.*, **30** (2022), 961–977. https://doi.org/10.3934/era.2022050

35. S. Li, G. Zhang, J. Wang, Y. Chen, B. Deng, Emergent central pattern generator behavior in chemical coupled two-compartment models with time delay, *Physica A*, **491** (2018), 177–187. https://doi.org/10.1016/j.physa.2017.08.121

36. A. Doloc-Mihu, R. L. Calabrese, A database of computational models of a half-center oscillator for analyzing how neuronal parameters influence network activity, *J. Biol. Phys.*, **37** (2011), 263–283. https://doi.org/10.1007/s10867-011-9215-y

37. A. Doloc-Mihu, R. L. Calabrese, Analysis of family structures reveals robustness or sensitivity of bursting activity to parameter variations in a half-center oscillator (HCO) model, *eNeuro*, **3** (2016). https://doi.org/10.1523/ENEURO.0015-16.2016

38. I. Elices, P. Varona, Asymmetry factors shaping regular and irregular bursting rhythms in central pattern generators, *Front. Comput. Neurosci.*, **11** (2017), 9. https://doi.org/10.3389/fncom.2017.00009

39. A. J. White, Sensory feedback expands dynamic complexity and aids in robustness against noise, *Biol. Cybern.*, **116** (2022), 267–269. https://doi.org/10.1007/s00422-021-00917-2

40. Z. Yu, P. J. Thomas, Dynamical consequences of sensory feedback in a half-center oscillator coupled to a simple motor system, *Biol. Cybern.*, **115** (2021), 135–160. https://doi.org/10.1007/s00422-021-00864-y

41. R. Huerta, P. Varona, M. I. Rabinovich, H. D. I. Abarbanel, Topology selection by chaotic neurons of a pyloric central pattern generator, *Biol. Cybern.*, **84** (2001), L1–L8. https://doi.org/10.1007/PL00007976

42. V. In, A. Kho, P. Longhini, J. D. Neff, A. Palacios, P. L. Buono, Meet ANIBOT: the first biologically-inspired animal robot, *Int. J. Bifurcation Chaos*, **32** (2022), 2230001. https://doi.org/10.1142/S0218127422300014

43. A. S. Lele, Y. Fang, J. Ting, A. Raychowdhury, Learning to walk: bio-mimetic hexapod locomotion via reinforcement-based spiking central pattern generation, *IEEE J. Emerging Sel. Top. Circuits Syst.*, **10** (2020), 536–545. https://doi.org/10.1109/JETCAS.2020.3033135

44. T. Sun, Z. Dai, P. Manoonpong, Distributed-force-feedback-based reflex with online learning for adaptive quadruped motor control, *Neural Networks*, **142** (2021), 410–427. https://doi.org/10.1016/j.neunet.2021.06.001

45. A. Espinal, H. Rostro-Gonzalez, M. Carpio, E. I. Guerra-Hernandez, M. Ornelas-Rodriguez, M. Sotelo-Figueroa, Design of spiking central pattern generators for multiple locomotion gaits in hexapod robots by christiansen grammar evolution, *Front. Neurorobot.*, **10** (2016), 6. https://doi.org/10.3389/fnbot.2016.00006

46. F. Zhan, S. Liu, Response of electrical activity in an improved neuron model under electromagnetic radiation and noise, *Front. Comput. Neurosci.*, **11** (2017), 107. https://doi.org/10.3389/fncom.2017.00107

47. F. Zhan, S. Liu, J. Wang, B. Lu, Bursting patterns and mixed-mode oscillations in reduced Purkinje model, *Int. J. Mod. Phys. B*, **32** (2018), 1850043. https://doi.org/10.1142/S0217979218500431

48. D. Terman, J. E. Rubin, A. C. Yew, C. J. Wilson, Activity patterns in a model for the subthalamopallidal network of the basal ganglia, *J. Neurosci.*, **22** (2002), 2963–2976. https://doi.org/10.1523/JNEUROSCI.22-07-02963.2002

49. F. Su, J. Wang, S. Niu, H. Li, B. Deng, C. Liu, et al., Nonlinear predictive control for adaptive adjustments of deep brain stimulation parameters in basal ganglia–thalamic network, *Neural Networks*, **98** (2018), 283–295. https://doi.org/10.1016/j.neunet.2017.12.001

50. J. Song, S. Liu, H. Lin, Model-based quantitative optimization of deep brain stimulation and prediction of Parkinson's states, *Neuroscience*, **498** (2022), 105–124. https://doi.org/10.1016/j.neuroscience.2022.05.019

51. J. Song, H. Lin, S. Liu, Basal ganglia network dynamics and function: role of direct, indirect and hyper-direct pathways in action selection, *Network: Comput. Neural Syst.*, **34** (2023), 84–121. https://doi.org/10.1080/0954898X.2023.2173816

52. M. Valero, I. Zutshi, E. Yoon, G. Buzsáki, Probing subthreshold dynamics of hippocampal neurons by pulsed optogenetics, *Science*, **375** (2022), 570–574. https://doi.org/10.1126/science.abm1891

53. C. A. Tassinari, G. Cantalupo, B. Hoegl, P. Cortelli, L. Tassi, S. Francione, et al., Neuroethological approach to frontolimbic epileptic seizures and parasomnias: the same central pattern generators for the same behaviours, *Rev. Neurol.*, **165** (2009), 762–768. https://doi.org/10.1016/j.neurol.2009.08.002

54. C. A. Tassinari, E. Gardella, G. Cantalupo, G. Rubboli, Relationship of central pattern generators with parasomnias and sleep-related epileptic seizures, *Sleep Med. Clin.*, **7** (2012), 125–134. https://doi.org/10.1016/j.jsmc.2012.01.003

AIMS Press